Journal of Rajasthan Academy of Physical Sciences
ISSN: 0972-6306; URL: http://raops.org.in
Vol.25, No.1&2, January-June, 2026, 66-89

EFFECT OF THERMAL RADIATION AND CHEMICAL REACTION ON MHD MICROPOLAR FLUID FLOW OVER AN EXPONENTIALLY CURVED STRETCHING SHEET

Bal Krishn Vaishnav[1], **Sushila Choudhary**[2*] and **Vijay Singh Maan**[3]
[1,2]Department of Mathematics, University of Rajasthan, Jaipur-302004, Rajasthan, India
[3]Manipal University Jaipur, Jaipur-303007, Rajasthan, India
E-mail: balkrishnvaishnav@gmail.com[1], vijay.maan@jaipur.manipal.edu[3]
sumathru11@gmail.com[2*]

Abstract : This article points out a numerical study of heat and mass transfer on an MHD Micropolar fluid that passes over an exponentially curved stretching sheet. The influence of thermal radiation and chemical reaction is also discussed. In this study, curvilinear coordinates are applied to describe the governing equations. By using suitable transformations, coupled non-linear ordinary differential equations are obtained with appropriate boundary conditions from the governing partial differential equations. "Bvp4c", a MATLAB solver, is used to get a numerical solution of the obtained non-linear ordinary differential equations. The impact of pertinent parameters used in the governing equations is evaluated graphically and explained in the results and discussion section. This investigation describes how heat and mass transfer are affected by the radius of curvature and the magnetic field. The findings demonstrate that increased curvature and magnetic intensity generally reduce the heat transfer rate at the wall, while higher values of the magnetic parameter led to expansion in the solutal boundary layer.

2010 Mathematics Subject Classification : 76Axx, 76Dxx, 76Sxx, 76Wxx, and 80Axx

Keywords : Micropolar fluid, Thermal Radiation, MHD, Curved Sheet, Porous Medium, Chemical Reaction.

1. Introduction

Micropolar fluids are fluids with microstructure belonging to a class of fluids with non-symmetrical stress tensors, referred to as polar fluids. Micropolar fluids are typically characterized by the presence of microscopic elements, such as randomly distributed particles, within a viscous base substance. These fluids play a significant role in various engineering and technological contexts, including applications in lubrication, polymer processing, colloidal systems, modeling blood circulation, refining petroleum, polymer manufacturing, centrifugal separation techniques, cooling tower operations, chemical process engineering, metal wire drawing, and solar energy technology. Sakiadis [32] primarily examined the boundary layer (BL) behaviour and showed that the motion of

continuous surfaces can be studied using the boundary layer theory and its basic equation. Eringen [9] defined Micropolar fluid, which exhibits some microstructural effect produced by its microstructure. In the presence of radiation, Hussain et al. [12] investigated the various features of Micropolar fluid that passes over a sheet that is permeable and stretched. Then, they solved it analytically using the HAM (Homotopy Analysis Method). Heat transfer properties for a Micropolar fluid that is flowing over a vertical stretching sheet in the presence of buoyancy force effect have been carried out by Abd El-Aziz [4]. This work was further extended by Mohanty et al. [19] to add mass transfer and porous media analysis. Hayat et al. [11] examined how Micropolar fluids behave as they move along a curved, stretched surface while considering the impact of heat being generated or absorbed within the flow. Shabbir et al. [35] investigated the heat transfer and dynamic properties of these fluids over curved sheets, employing the Keller Box method for their analysis. Pasha et al. [25] utilized numerical approaches to analyze the fundamental characteristics of Micropolar fluids in porous environments, specifically applying both the Variation Iteration Method (VIM) and the Adomian Decomposition Method (ADM) to assess heat transport behavior.

Exponentially curved stretching sheet is a fluid mechanics and materials science concept, characterized by their unique geometry and behavior under various forces. These sheets are designed with a curvature that increases exponentially, significantly influencing the flow of fluids around them and their mechanical properties. Curved sheets play an important role in many sectors of engineering and manufacturing processes. This sheet has several uses, including the manufacture of rubber sheets, hot rolling, wire drawing, glass puffing, extrusion operations, condensation of metallic plates, and crystal creation, aerospace engineering, microfluidics, biomedical devices, textile engineering, robotics. Magnetohydrodynamics (MHD) focuses on examining the motion and properties of electrically conducting fluids when subjected to magnetic fields. It integrates concepts from fluid mechanics and electromagnetism to explain the interaction between the fluid and magnetic forces, resulting in distinct behaviors and phenomena. MHD is used in various fields of fusion energy, astrophysics, electromagnetic pumps, metallurgy, environmental engineering, medicine, etc. Char and Chang [8] explored the laminar free convection flow of Micropolar fluids along a curved surface and solved the problem using the cubic spline collocation method for numerical analysis. Sajid et al. [30] worked on the curved stretching sheet and concluded that pressure can’t be neglected inside the boundary layer for a curved stretching sheet, and away from the boundary, it tends to be zero. Sajid et al. [30] investigated the flow of Micropolar fluid over curved stretching sheet. Heat transfer characteristics over a curved stretching surface under the influence of a magnetic field have been investigated by Abbas et al. [1]. Micropolar flow pattern over a curved stretched/shrunk surface has been investigated by Saleh et al. [33], who concluded that in the case of the increasing radius of curvature (k), the couple stress factor decreases in weak concentration ($m = 0.5$) while it increases in strong concentration ($m = 0$). The behavior of Casson fluid, whenever it passes over a curved stretchable sheet, has been analyzed by Nagaraja and Gireesha [22]. In this investigation, they use the boundary condition as a convective mass and heat flux. Kumar et al. [18] studied the dynamics of Micropolar fluid

flowing over a curved, stretchable surface. Kumar et al. [17] analyzed Casson fluid behavior on an exponentially curved stretching sheet, applying the shooting method combined with the Runge-Kutta fourth-order technique for solving the flow equations. Qian et al. [26] investigated heat transfer characteristics of magnetohydrodynamic (MHD) Micropolar fluid across an exponentially extending curved surface, factoring in Ohmic heating as well as heat sources and sinks using the Keller Box method. Ahmed et al. [5] examined the influence of thermal radiation on MHD Williamson nanofluid flow over a similar curved, stretchable surface. Jawad et al. [15] conducted a magnetohydrodynamic nanofluid flow study over an exponentially stretching curved surface, utilizing the Homotopy Analysis Method (HAM) to obtain solutions. Abbas et al. [2] performed a theoretical study on non-Newtonian micropolar nanofluid dynamics over an exponentially stretching surface affected by free stream velocity. More recently, Nabwey et al. [21] analyzed heat transfer in MHD flow of Carreau ternary-hybrid nanofluid, composed of titanium oxide, aluminum oxide, and silver nanoparticles dispersed in water, over an exponentially stretched curved surface using Bvp4c. Abbas et al. [3] further investigated the thermodynamics of Casson-Sutterby Micropolar fluid flow along an exponentially stretching curved sheet, incorporating MHD effects and heat generation at low Reynolds numbers. Chandrakala and Rao [7] studied the influence of magnetohydrodynamics on mixed convective hybrid nanofluids, which are formed by Copper (Cu) and metal oxide (Al_2O_3), flowing over an exponentially stretching sheet.

Thermal radiation is the emission of electromagnetic waves from the surface of an object due to its temperature. All bodies emit thermal radiation, and the amount and wavelength of the radiation depend on the temperature and emissivity of the surface. This phenomenon is described by Planck's law, Stefan-Boltzmann law, and Wien's displacement law, and it plays a crucial role in heat transfer processes. Thermal radiation is used in various fields of thermal management, thermal imaging, spacecraft design, solar energy, climate science, and heating systems. Hayat et al. [10] examined how thermal radiation and chemical reactions influence magnetohydrodynamic (MHD) convective flow past a curved surface. Later, Jamshed et al. [14] studied the combined effects of thermal radiation and entropy generation on Casson nanofluid flow over a stretching sheet, employing the Keller-Box method under slip boundary conditions and incorporating solar thermal transport. Similarly, Oke et al. [24] explored the role of Coriolis force and radiative heat transfer in the behavior of water-based hybrid nanofluids flowing over an exponentially stretching plate. Furthermore, Murtaza et al. [20] examined how magnetohydrodynamics influences the flow of water-based nanofluids across a permeable exponentially shrinking sheet, particularly in the presence of thermal radiation effects. Zeeshan et al. [41] further analyzed how nanofluids and hybrid nanofluids enhance thermal conductivity over an exponentially curved stretching surface, accounting for melting effects and second-order slip conditions. More recently, Sanni et al. [34] investigated heat and mass transfer of an advection-diffusion viscous fluid across a magnetized curved stretching sheet under the combined influence of thermal radiation and chemical reactions, solving the problem with the Keller-Box shooting technique coupled with Jacobi's iterative scheme.

Chemical reactions are processes in which reactant substances are converted into new products by the breaking of existing chemical bonds and the formation of new ones. These reactions can be grouped into several categories, such as synthesis, decomposition, single displacement, double displacement, and combustion reactions. Thermal radiation is used in various fields of pharmaceuticals, energy production, agriculture, material science, food industry, environmental science, cosmetics and personal care, and electrochemistry. Mass and heat transfer characteristics of Casson fluid flow with chemical reaction and viscous dissipation have been carried out by Raju et al. [27] and solved using the Bvp4c MATLAB package. They also included the effect of the uniform magnetic field in this consideration. Mass and heat transfer of Casson Micropolar fluid flow in a porous media has been carried out by Amjad et al. [6] and solved this flow pattern with the help of Bvp4c MATLAB code. Islam et al. [13] examined the entropy optimization problem with the help of the Homotopy Analysis Method (HAM). In the presence of viscous dissipation and chemical reaction, the trend of temperature and concentration profile with various parameters in the exponentially permeable stretched surface has been discussed by Reddy et al. [29]. In this study, they considered the surface as a permeable curved stretching surface. In the presence of a magnetic effect, viscous dissipation, and activation energy, heat and mass characteristics of micropolar nanofluid have been discussed by Khan et al. [16]. Sidahmed et al. [37] investigated the impact of chemical reactions for viscoelastic flow over an exponentially stretching sheet on the Cattaneo-Christov heat flux model and solved this problem using the analytical Straight-Line Method (SLM). The study on MHD flow of micropolar fluid is given by Naved et al. [23], Rees and Bassom [28], Yasmin et al. [38]. Hybrid nano fluid is studied by Zaianl et al. [39] and Zangooee et al. [40]

The present study focuses on the thermal radiation effect on MHD Micropolar fluid flow over an exponentially stretched curved surface in the presence of a chemical reaction. Controlled thermal radiation is important for a broad range of applications, including polymer processing, spectroscopy, optoelectronics, and energy conversion devices. The governing set of partial differential equations is trans- formed into nonlinear ordinary differential equations through suitable similarity transformations. These reduced equations are then solved using the Bvp4c solver in MATLAB. The influence of various physical parameters on dimensionless velocity, temperature, microrotation, and concentration distributions is analyzed and presented using graphical and tabular illustrations.

2. Mathematical Formulation

Consider the steady 2-D boundary layer and an incompressible flow of Micropolar fluid under the influence of a magnetic field and thermal radiation, over a curved stretching sheet in a porous medium. Two equal and opposite forces are applied along and perpendicular to the s-and r-directions, respectively, so that the sheet is stretched keeping the origin fixed, which is shown in Figure 1. The stretching velocity of the surface is $u = ae^{s/L}$ where ($a > 0$) is a constant. A constant magnetic field B_0 is assumed to be

applied in the r-direction. Under above assumptions, the governing equations are (Shi et.al. [36]) given as follows:

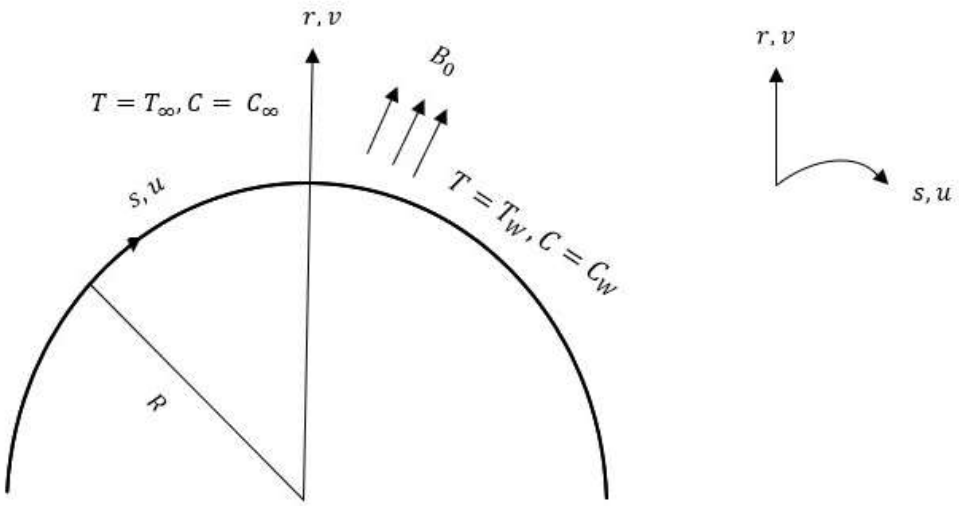

Fig. 1: Graphical representation of the flow problem

$$\frac{\partial (r+R)v}{\partial r} + R\frac{\partial u}{\partial s} = 0 \ , \tag{1}$$

$$\frac{u^2}{(r+R)} = \frac{1}{\rho}\frac{\partial p}{\partial r} \ , \tag{2}$$

$$v\frac{\partial u}{\partial r} + \frac{Ru}{(r+R)}\frac{\partial u}{\partial s} + \frac{uv}{(r+R)} = -\frac{1}{\rho}\frac{R}{(r+R)}\frac{\partial p}{\partial s} + \left(\nu + \frac{k'}{\rho}\right)$$
$$\left(\frac{\partial^2 u}{\partial r^2} + \frac{1}{(r+R)}\frac{\partial u}{\partial r} - \frac{u}{(r+R)^2}\right) - \frac{k'}{\rho}\frac{\partial N}{\partial r} - \frac{\sigma B^2}{\rho}u - \frac{\nu}{k_p}u, \tag{3}$$

$$v\frac{\partial N}{\partial r} + \frac{Ru}{(r+R)}\frac{\partial N}{\partial s} = \frac{\gamma}{\rho j}\left(\frac{\partial^2 N}{\partial r^2} + \frac{1}{(r+R)}\frac{\partial N}{\partial r}\right) - \left(\frac{k'}{\rho j}\right)\left(2N + \frac{\partial u}{\partial r} + \frac{u}{(r+R)}\right), \tag{4}$$

$$\rho C_p\left(v\frac{\partial T}{\partial r} + \frac{Ru}{(r+R)}\frac{\partial T}{\partial s}\right) = \kappa\left(\frac{\partial^2 T}{\partial r^2} + \frac{1}{(r+R)}\frac{\partial T}{\partial r}\right) - \frac{1}{(r+R)}\frac{\partial (r+R)q_r}{\partial r} + \tag{5}$$

$$(\mu + k')\left(\frac{\partial u}{\partial r} - \frac{u}{(r+R)}\right)^2, \tag{6}$$

$$v\frac{\partial C}{\partial r} + \frac{Ru}{(r+R)}\frac{\partial N}{\partial s} = D\left(\frac{\partial^2 C}{\partial r^2} + \frac{1}{(r+R)}\frac{\partial C}{\partial r}\right) - K_r(C - C_\infty), \tag{7}$$

Here, u and v denote the fluid velocity components along the s- and r- directions, respectively. The symbol ρ represents the fluid density, while μ is the kinematic viscosity and p the pressure. The microrotation is indicated by N, and j denotes the microinertia per unit mass. The vortex viscosity is given by k', whereas κ corresponds to the thermal conductivity. The coefficient of mass diffusion is denoted by D, and T denotes the fluid temperature. The specific heat at constant pressure is denoted by C_p, with q_r representing the radiative heat flux. The chemical reaction rate is symbolized as K_r. Here, T_w indicates the surface temperature, and $T\infty$ is the ambient (free-stream) temperature. Similarly, C stands for concentration, with C_w as the concentration at the sheet and C_∞ as the concentration far from the surface. The microrotation boundary condition is governed by the parameter m, which ranges from 0 to 1; specifically, m = 0.0 corresponds to a strong concentration, m = 0.5 to a moderate concentration, and m = 1.0 to a weak concentration case.

The spin gradient viscosity is denoted by γ, which is defined as (Saleh et al. [34])

$\gamma = \left(\mu + \frac{k'}{2}\right)j = \mu\left(1 + \frac{C_1}{2}\right)j$, where $C_1 = \frac{k'}{\mu}$ is the material parameter and $j = \frac{2\nu L}{ae^{\frac{s}{L}}}$, where L the reference length.

Using the Rosseland estimation, the radiative heat flux q_r is defined as (Hussain et. al. [12]) $q_r = -\frac{16\sigma^* T_\infty^3}{3k^*}\frac{\partial T}{\partial r}$, using this expression, equation (5) can be written as

$$\rho C_p\left(v\frac{\partial T}{\partial r} + \frac{Ru}{(r+R)}\frac{\partial T}{\partial s}\right) = \kappa\left(\frac{\partial^2 T}{\partial r^2} + \frac{1}{(r+R)}\frac{\partial T}{\partial r}\right) - \frac{1}{(r+R)}\frac{\partial (r+R)q_r}{\partial r} + (\mu + k')\left(\frac{\partial u}{\partial r} - \frac{u}{(r+R)}\right)^2, \tag{8}$$

3. Method of Solution

The following similarity variables are considered here (Shi et al. [36] and Hayat et al. [10])

$$u = ae^{\frac{s}{L}} f'(\eta), \quad v = -\frac{R}{r+R}\sqrt{\frac{a\nu e^{\frac{s}{L}}}{2L}}\left(f(\eta)+\eta f'(\eta)\right), \quad N = ae^{\frac{s}{L}}\sqrt{\frac{ae^{\frac{s}{L}}}{2\nu L}}g(\eta),$$

$$k = \sqrt{\frac{ae^{\frac{s}{L}}}{2\nu L}}R,$$

$$\eta = \sqrt{\frac{ae^{\frac{s}{L}}}{2\nu L}}r, \quad p = \rho a^2 e^{\frac{2s}{L}} P(\eta), \quad \theta(\eta) = \frac{T-T_\infty}{T_w-T_\infty}, \quad \phi(\eta) = \frac{C-C_\infty}{C_w-C_\infty}. \tag{9}$$

Using these transformations, equation (1) is identically satisfied. The governing equations (2), (3), (4), (6) and (8), using similarity transformations, reduced the non-linear ODE as follows:

$$\frac{\partial P}{\partial \eta} = \frac{f'^2}{\eta+k}, \tag{10}$$

$$\frac{2k}{\eta+k}P(\eta) = (1+C_1)\left(f'''+\frac{f''}{\eta+k}-\frac{f'}{(\eta+k)^2}\right)-C_1 g'-(Ma+K_p)f'-\frac{k}{\eta+k}\left(f'^2-ff''-\frac{ff'}{\eta+k}\right) \tag{11}$$

Now eliminating P between (10) and (11), we get equation (12) as follows;

$$\begin{aligned}&(1+C_1)\left(f''''+\frac{2f'''}{\eta+k}-\frac{f''}{(\eta+k)^2}+\frac{f'}{(\eta+k)^3}\right)-\frac{k}{\eta+k}(3f'f''-ff''')-\frac{k}{(\eta+k)^2}(3f'^2-ff'')\\&-\frac{k}{(\eta+k)^3}ff'-C_1\left(g''+\frac{g'}{\eta+k}\right)-(Ma+K_p)\left(f''+\frac{f'}{\eta+k}\right)=0\end{aligned} \tag{12}$$

$$\left(1+\frac{C_1}{2}\right)\left(g''+\frac{g'}{\eta+k}\right)+\frac{k}{\eta+k}(fg'-3f'g)-C_1\left(2g+f''+\frac{f'}{\eta+k}\right)=0 \tag{13}$$

$$(1+Nr)\left(\theta''+\frac{\theta'}{\eta+k}\right)+\frac{k}{\eta+k}\Pr(f\theta'-2f'\theta)+\Pr Ec(1+C_1)\left(f''-\frac{f'}{\eta+k}\right)^2=0 \tag{14}$$

$$\phi''+\frac{\phi'}{\eta+k}+\frac{k}{\eta+k}Sc(f\phi'-2f'\phi)-Sc\ Cr\ \phi=0 \tag{15}$$

The corresponding transformed boundary conditions are

$$\begin{cases} f=0,\ f'=1,\ g=-mf'',\ \theta=1,\ \phi=1 & \text{at}\quad \eta=0, \\ f'\to 0,\ f''\to 0,\ g\to 0,\ \theta\to 0,\ \phi\to 0, & \text{as}\ \eta\to\infty. \end{cases} \tag{16}$$

Here K_p is the permeability parameter, Ma is the magnetic parameter, $\Pr$ is the Prandtl number, Nr is the thermal radiation parameter, Cr is the chemical reaction parameter, Sc is the Schmidt number, C_1 is the material parameter, k is the radius of curvature. These parameters are further defined as

$$K_p=\frac{2\nu L}{ak_p e^{\frac{s}{L}}},\quad Nr=\frac{16\sigma^* T_\infty^3}{3k^*\kappa},\quad k=\sqrt{\frac{ae^{\frac{s}{L}}}{2\nu L}}R,\quad Ma=\frac{2\sigma B_0^2 L}{\rho a},\quad Sc=\frac{\nu}{D},$$

$$Ec=\frac{u_w^2}{C_p\left(T_w-T_\infty\right)},\ \Pr=\frac{\mu C_p}{\kappa},\ C_1=\frac{k'}{\mu},\ Cr=\frac{2LK_r}{ae^{\frac{s}{L}}}. \tag{17}$$

The system of non-linear coupled ordinary differential equations (12) to (15), along with the boundary conditions specified in (16), is addressed using the bvp4c MATLAB function. In this approach, an initial guess for any unknown parameters is provided through the Solinit parameters. The bvp4c solver then provides the final values of these parameters in sol-parameters. This technique yields a solution that is continuous over the specified interval and possesses a continuous first-order derivative within that range. The method solves a set of first-order differential equations, which involves converting the higher-order, non-linear ordinary differential equations from (12) to (15) into a system of first-order, simultaneous, non-linear differential equations.

Let $f=f_1,\ f'=f_2,\ f''=f_3,\ f'''=f_4,\ g=f_5,\ g'=f_6,\ \theta=f_7,\ \theta'=f_8,\ \phi=f_9$, and $\phi'=f_{10}$.

Then we get the following system of first-order differential equations:

$$f_1'=f_2,\ f_2'=f_3,\ f_3'=f_4,$$

$$f_4'=\frac{1}{(1+C_1)}\left\{\begin{aligned}&\frac{k}{\eta+k}\left(3f_2f_3-f_1f_4\right)+\frac{k}{(\eta+k)^2}\left(3f_2^2-f_1f_3\right)+\frac{k}{(\eta+k)^3}f_1f_2\\&+\frac{2C_1}{(2+C_1)}\left[\frac{k}{\eta+k}\left(3f_2f_5-f_1f_6\right)+C_1\left(2f_5+f_3+\frac{f_2}{\eta+k}\right)\right]+\left(Ma+K_p\right)\left(f_3+\frac{f_2}{\eta+k}\right)\end{aligned}\right\}$$

$$-\frac{2f_4}{(\eta+k)}+\frac{f_3}{(\eta+k)^2}-\frac{f_2}{(\eta+k)^3}$$

$$f_5' = f_6,$$

$$f_6' = \frac{2C_1}{(2+C_1)}\left[\frac{k}{\eta+k}(3f_2f_5 - f_1f_6) + C_1\left(2f_5 + f_3 + \frac{f_2}{\eta+k}\right)\right] - \frac{f_6}{\eta+k},$$

$$f_7' = f_8,$$

$$f_8' = -\frac{1}{(1+Nr)}\left[\frac{k}{\eta+k}\Pr(f_1f_8 - 2f_2f_7) + \Pr Ec(1+C_1)\left(f_3 - \frac{f_2}{(\eta+k)}\right)^2\right] - \frac{f_8}{\eta+k},$$

$$f_9' = f_{10},$$

$$f_{10}' = \frac{k}{\eta+k}Sc(2f_2f_9 - f_1f_{10}) + Sc\ Cr\ f_9 - \frac{f_{10}}{\eta+k}. \tag{18}$$

and corresponding boundary conditions reduced to

$$\begin{cases} f_1 = 0,\ f_2 = 1,\ f_5 = -mf_3,\ f_7 = 1,\ f_9 = 1, & \text{at } \eta=0, \\ f_2 \to 0,\ f_3 \to 0,\ f_5 \to 0,\ f_7 \to 0,\ f_9 \to 0, & \text{as } \eta \to \infty. \end{cases} \tag{19}$$

In this case, a step size of $\Delta\eta = 0.01$ was used, with an error tolerance of $(10)^{-3}$. The results were obtained with accuracy up to four decimal places. Although the boundary conditions are specified for $\eta \to \infty$ the graph asymptotically approaches the η axis after a certain value of η. Consequently, $\eta = 10$ was used in place of $\eta \to \infty$.

4. Relevant Physical Measures

The primary physical parameters (Shabbir et al. [36]) are outlined below:

The local skin friction coefficient is given by

$$C_{fs}(\mathrm{Re}_s)^{\frac{1}{2}} = \frac{\tau_{rs}}{\rho u_w^2} = \frac{1}{\sqrt{2}}\left\{\left[1+(1-m)C_1\right]f''(0) - (1+C_1)\frac{f'(0)}{k}\right\}, \tag{20}$$

where $\tau_{rs} = \left\{(\mu+k')\left(\frac{\partial u}{\partial r} - \frac{u}{(r+R)}\right) + k'N\right\}_{r=0}$ is the wall shear stress at the surface.

The local Nusselt number is given by

$$Nu_s\left(\mathrm{Re}_s\right)^{-\frac{1}{2}} = \frac{Lq_w}{\kappa\left(T_w - T_\infty\right)} = -\frac{1}{\sqrt{2}}\left(1+Nr\right)\theta'\left(0\right), \tag{21}$$

where $q_w = -\left(\kappa + \frac{16\sigma^* T_\infty^3}{3k^*}\right)\left(\frac{\partial T}{\partial r}\right)_{r=0}$ is the heat flux at the surface.

The couple stress factor is given by

$$C_m = \frac{M_w}{\mu j u_w} = \left(1+\frac{C_1}{2}\right)g'\left(0\right), \tag{22}$$

where $M_w = \gamma\left(\frac{\partial N}{\partial r}\right)_{r=0}$ is the couple stress at the surface.

The local Sherwood number is given by

$$Sh_s\left(\mathrm{Re}_s\right)^{-\frac{1}{2}} = \frac{Lq_m}{D\left(C_w - C_\infty\right)} = -\frac{1}{\sqrt{2}}\phi'\left(0\right), \tag{23}$$

where $q_m = -D\left(\frac{\partial C}{\partial r}\right)_{r=0}$ is the mass flux at the surface.

Here $\mathrm{Re}_w = \frac{u_w L}{\nu}$ is local Reynolds number.

5. Results and Discussion

The system of nonlinear coupled ordinary first-order differential equations presented in (18), along with the boundary conditions given in (19), has been solved using MATLAB's bvp4c solver. The influence of the governing parameters involved in the problem has then been examined with the magnetic parameter (*Ma*), permeability parameter (*Kp*), material parameter (C_1), microrotation parameter (*m*), thermal radiation parameter (*Nr*), radius of curvature (*k*), Prandtl number (Pr), Eckert number (*Ec*), Schmidt number (*Sc*) and chemical reaction parameter (*Cr*) has been shown through graphs and tables. We assumed the common values of dimensionless parameters for computing the problem as $Ma = 1.5$, $C_1 = 4.0$, $Nr = 1.0$, $Kp = 1.0$, $m = 0.5$, $\mathrm{Pr} = 9.0$, $Ec = 0.3$, $Sc = 1.2$, $Cr = 1.0$, $k = 6.0$, unless otherwise specified. The obtained results are displayed through graphs and tables. For cumulative values of the magnetic parameter *Ma*, the variations in the velocity, temperature, microrotation, and concentration profiles are shown in figures 2-6. Since the Lorentz force opposes the flow, the velocity (here $f(\eta)$ and $f'(\eta)$ are the velocities in the direction of *y* and *x*,

respectively) profile decreases with the increasing values of Ma, which is displayed in figures 2 and 3 respectively. It is detected in figure 4 that initially the microrotation profile boosts up with the enhanced values of Ma but after $\eta = 2.02636$, it shows decreasing behavior. In figure 5, owing to the Lorentz force, which generates some heat, therefore the temperature profile rises with the rising values of Ma but after $\eta = 1.6$, the opposite scenario can be seen, because of the high Prandtl Number $\Pr$. It is shown in figure 6 that the concentration profile increases as the boosting values of Ma. For assorted values of the permeability parameter (Kp), changing velocity, temperature, and microrotation patterns are displayed in figures 7-10. Now, it is perceived from figures 7-8 that the velocity profile declines as the value of Kp enhances. Physically, the medium's permeability reduces with decreasing values of Kp which causes the fluid velocity to increase. Furthermore, It is observed from figures 9 and 10 that temperature and microrotation profiles increase near the surface, but after $\eta = 1.615$ and $\eta = 2.10$ respectively, it is reduced for increasing values of Kp. Figures 11-15 demonstrate the properties of the velocity, temperature, microrotation, and concentration profiles for various material parameter values C_1. Now, it is discerned from figures 11-14 that the pattern of the velocity and temperature profiles is enhanced with boosting values of C_1 while the opposite scenario is seen for the concentration profile. The microrotation of the fluid increases with the increasing value of C_1, velocity increases as a result. It is inspected from figure 15 that for rising values of C_1, the microrotation profile near the surface reduces but increases away from the surface, where the crossing point is $\eta = 1.744$. The effect of the radius of curvature k on velocity, temperature, and microrotation profiles is displayed in figures 16-19. Furthermore, we can see from figures 16-18 that, characteristics of velocity profiles are proportional to assorted values of k while the opposite trend is seen for the microrotation profile. Now, from figure 19, the behavior of the microrotation profile near the surface reduces for an enhancing value of k but after $\eta = 0.35$, it increases. Figures 20-23 indicate the changing trend of velocity, temperature, and microrotation profiles for variation of microrotation parameter m. Figures 20-22 shows that the velocity profile increases as m is raised while near the surface opposite behavior is seen for temperature distribution but after $\eta = 1.04$ proportional behavior can be seen. Furthermore, in figure 23 microrotation profile is increasing as values of m rise. The sketched graph in figure 24 shows the temperature profile for different values of radiation parameter Nr. Radiation is really a thermal transference phenomenon that transmits heat via liquid particles. As a result, the flow of

heat is produced. Therefore, at larger values of Nr, we see a rise in the thermal boundary layer thickness. Figure 25 is sketched to show the effect of Eckert number Ec on a rising temperature pattern. It can be observed that the rising Ec leads to growing temperature trends, because, with increasing values of Ec, the Kinetic Energy of the fluid flow increases, which causes to rise in the temperature distribution. Heat pattern how is affected by Prandtl number $\Pr$ is presented in figure 26. Owing to the inverse relation between $\Pr$ number and boundary layer thickness, increasing values of $\Pr$, decreasing behavior is detected for the temperature profile. Figure 27 illustrates the concentration profile shows the depreciate characteristics for accelerated values of Schmidt number Sc due to the fact that as Sc rises, more Brownian diffusion occurs for Micropolar fluid, therefore decreasing the concentration profiles. For enhancing values of the Chemical reaction parameter Cr changing trends of the solutal profile are given in figure 28. The increase in reactive agents to a decrease in chemicals causes to decrease solutal boundary layer profile.

The impact of various parameters Ma, Kp, k, C_1, and m to the skin friction coefficient is given in Table 1. From this table, we concluded that the Skin friction coefficient shows rising behavior for elevating values of C_1, and m while for enhancing values of Ma, Kp, and k opposite trend is obtained. Table 2 is made to compute the variation in Wall couple stress for diverse values of the parameters Ma, Kp, k, C_1 and m. As using the result in Table 2, we observed that wall couple stress improves when the values of parameters Ma, Kp, C_1 and m rise whereas declined for boosting values of k. Table 3 is formed to know how the Nusselt number is affected by various values of the parameters Ma, Kp, k, C_1, m, $\Pr$, $\Pr$, and Ec. It is seen that the Nusselt number rises with the values of k, m, Nr, and $\Pr$ whereas decreases with the values of Ma, Kp, C_1, and Ec. The influence of the parameters Ma, Kp, k, C_1, m, Sc and Cr on the Sherwood number are demonstrated in Table 4. By using data from this table, we can see that the Sherwood number shows the same behavior for Ma, Kp and k while reverse characteristics are seen for C_1, m, Sc and Cr.

6. Conclusions

In this article, mass and heat transfer are discussed for an MHD Micropolar fluid that is flowing over an exponentially curved stretching sheet. In this article, the effect of thermal radiation and chemical reactions is also considered. Bvp4c MATLAB solver is used to

find the thermal boundary layer thickness and solutal boundary layer thickness. Some obtained results are given as follows:

i. The velocity profile decreases for all values of η while the temperature profile near the surface increases, but far away from the surface decreases with the larger values of the magnetic parameter Ma, due to the Lorentz force and the high Prandtl Number Pr.

ii. With the progressive values of the Prandtl number Pr, thermal boundary layer thickness drops. In the heat transfer system, Pr may be controlled by the relative thickness of the thermal and momentum boundary layer. It can also be used in the field of fluid metal reactors.

iii. The micronation profile falls near the surface but uplifts far away from the surface with the enlarged values of the radius of curvature k. The radius of curvature plays a significant role in the field of physics and mathematics, such as the optical design of spherical lenses and mirrors, and differential geometry.

iv. The concentration profile is inversely affected by the Schmidt number Sc and chemical reaction parameter $C\mathrm{r}$.

This theoretical framework finds wide-ranging applications across various fields such as industrial innovation, biological transport systems, drying processes, high temperature plasma dynamics, astronomy, geophysics, sensor technology, and earthquake analysis. Additionally, it plays a significant role in energy production sectors, including thermal, hydroelectric, and nuclear power plants.

Table 5.1: Values of $\sqrt{2}\left(\mathrm{Re}_s\right)^{\frac{1}{2}} C_{fs}$ for Ma, Kp, k, C_1 and m.

Ma	Kp	k	C_1	m	$\{1+(1-m)C_1\} f''(0) -(1+C_1)\frac{f'(0)}{k}$
1.9	1.0	6.0	4.0	0.5	-1.6569616
3.7	1.0	6.0	4.0	0.5	-2.1372586
1.5	0.4	6.0	4.0	0.5	-1.3436869
1.5	0.8	6.0	4.0	0.5	-1.4742451
1.5	1.0	2.0	4.0	0.5	-0.2065664
1.5	1.0	4.0	4.0	0.5	-1.1823298
1.5	1.0	6.0	2.9	0.5	-1.5584631
1.5	1.0	6.0	3.8	0.5	-1.5403864
1.5	1.0	6.0	4.0	0.5	-1.5367579
1.5	1.0	6.0	4.0	0.9	-0.1069081

Table 5.2: Values of $-C_m$ for Ma, Kp, k, C_1 and m.

Ma	Kp	k	C_1	m	$-\left(1+\frac{C_1}{2}\right)g'(0)$
1.9	1.0	6.0	4.0	0.5	1.4052189
3.7	1.0	6.0	4.0	0.5	1.6950744
1.5	0.4	6.0	4.0	0.5	1.2267381
1.5	0.8	6.0	4.0	0.5	1.3000287
1.5	1.0	2.0	4.0	0.5	2.1045366
1.5	1.0	4.0	4.0	0.5	1.5124704
1.5	1.0	6.0	2.9	0.5	1.3106199
1.5	1.0	6.0	3.8	0.5	1.3296042
1.5	1.0	6.0	4.0	0.5	1.3356804
1.5	1.0	6.0	4.0	0.9	2.6733645

Table 5.3: Values of $-(1+Nr)\theta'(0)$ for Ma, Kp, k, C_1, m, $\Pr$, Nr and Ec.

Ma	Kp	k	C_1	m	$\Pr$	Nr	Ec	$-(1+Nr)\theta'(0)$
1.9	1.0	6.0	4.0	0.5	0.9	1.0	0.3	3.089494
3.7	1.0	6.0	4.0	0.5	0.9	1.0	0.3	2.157764
1.5	0.4	6.0	4.0	0.5	0.9	1.0	0.3	3.671998
1.5	0.8	6.0	4.0	0.5	0.9	1.0	0.3	3.431736
1.5	1.0	2.0	4.0	0.5	0.9	1.0	0.3	0.089478
1.5	1.0	4.0	4.0	0.5	0.9	1.0	0.3	2.623262
1.5	1.0	6.0	2.9	0.5	0.9	1.0	0.3	3.509842
1.5	1.0	6.0	3.8	0.5	0.9	1.0	0.3	3.344932
1.5	1.0	6.0	4.0	0.5	0.9	1.0	0.3	3.315640
1.5	1.0	6.0	4.0	0.9	0.9	1.0	0.3	3.764398
1.5	1.0	6.0	4.0	0.5	4.0	1.0	0.3	2.391164
1.5	1.0	6.0	4.0	0.5	6.0	1.0	0.3	2.821550
1.5	1.0	6.0	4.0	0.5	0.9	1.9	0.3	4.147348
1.5	1.0	6.0	4.0	0.5	0.9	3.5	0.3	5.380119
1.5	1.0	6.0	4.0	0.5	0.9	1.0	0.1	5.405490
1.5	1.0	6.0	4.0	0.5	0.9	1.0	0.3	3.315640

Table 5.4: Values of $-\phi'(0)$ for Ma, Kp, k, C_1, m, Sc and Cr.

Ma	Kp	k	C_1	m	Sc	Cr	$-\phi'(0)$
1.9	1.0	6.0	4.0	0.5	1.2	1.0	1.9717831
3.7	1.0	6.0	4.0	0.5	1.2	1.0	1.9474412
1.5	0.4	6.0	4.0	0.5	1.2	1.0	1.9881722
1.5	0.8	6.0	4.0	0.5	1.2	1.0	1.9812955
1.5	1.0	2.0	4.0	0.5	1.2	1.0	2.0699960
1.5	1.0	4.0	4.0	0.5	1.2	1.0	2.0017236
1.5	1.0	6.0	2.9	0.5	1.2	1.0	1.9612218
1.5	1.0	6.0	3.8	0.5	1.2	1.0	1.9754334
1.5	1.0	6.0	4.0	0.5	1.2	1.0	1.9780261
1.5	1.0	6.0	4.0	0.9	1.2	1.0	1.9914579
1.5	1.0	6.0	4.0	0.5	0.8	1.0	1.6025495
1.5	1.0	6.0	4.0	0.5	1.6	1.0	2.2953095
1.5	1.0	6.0	4.0	0.5	1.2	1.0	1.9780261
1.5	1.0	6.0	4.0	0.5	1.2	3.0	2.5562885

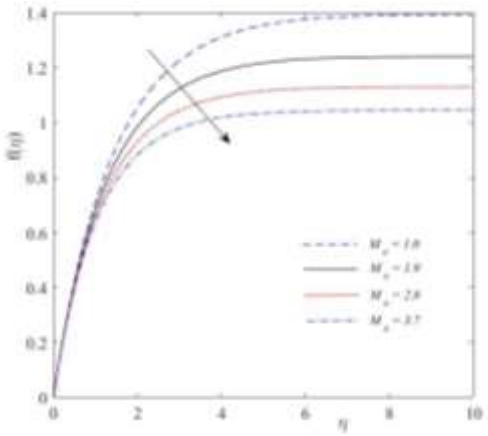

Fig. 2: Variation of $f(\eta)$ with Ma.

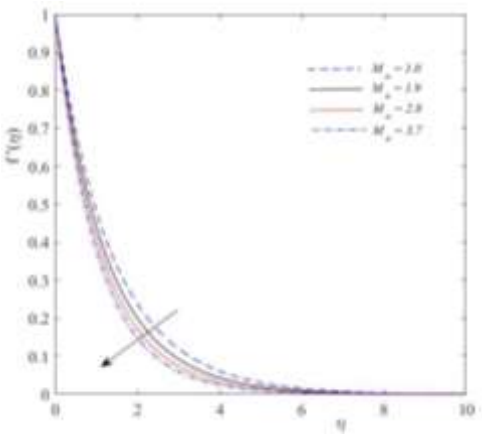

Fig. 3: Variation of $f'(\eta)$ with Ma.

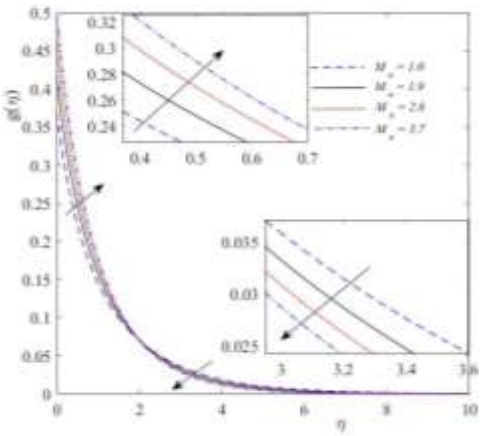

Fig. 4: Variation of $g(\eta)$ with Ma.

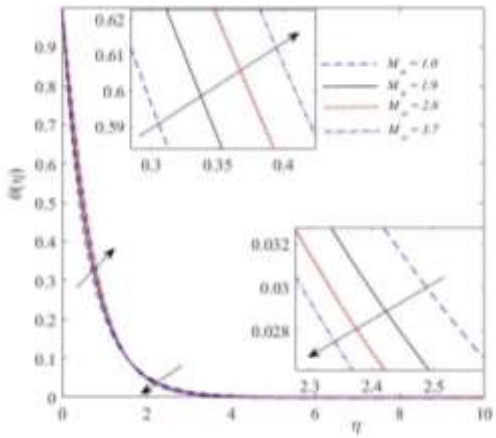

Fig. 5: Variation of $\theta(\eta)$ with Ma.

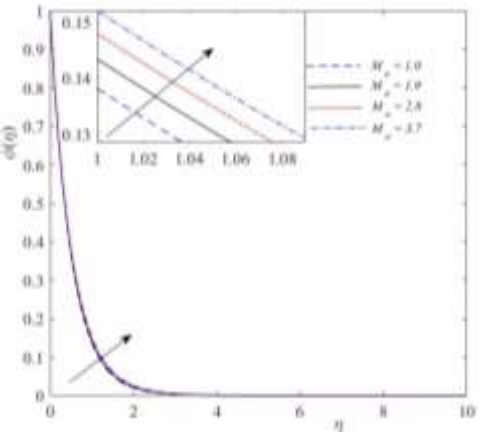

Fig. 6: Variation of $\phi(\eta)$ with Ma.

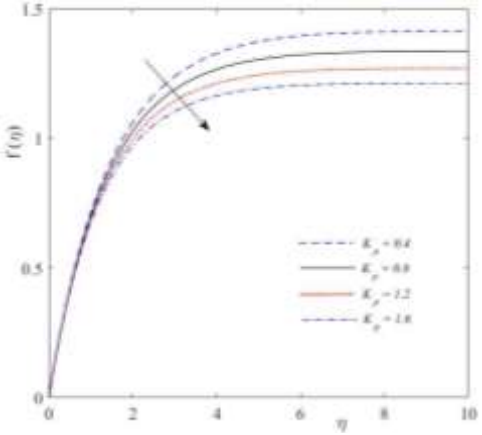

Fig. 7: Variation of $f(\eta)$ with Kp.

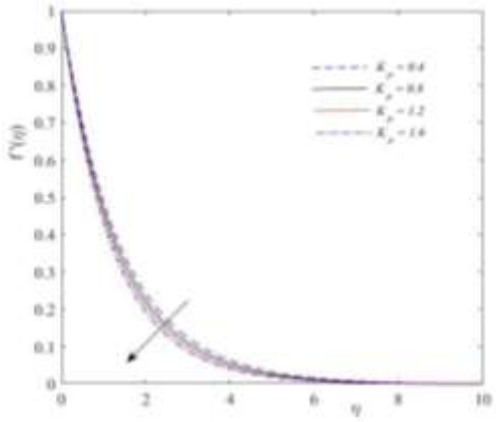

Fig. 8: Variation of $f'(\eta)$ with Kp.

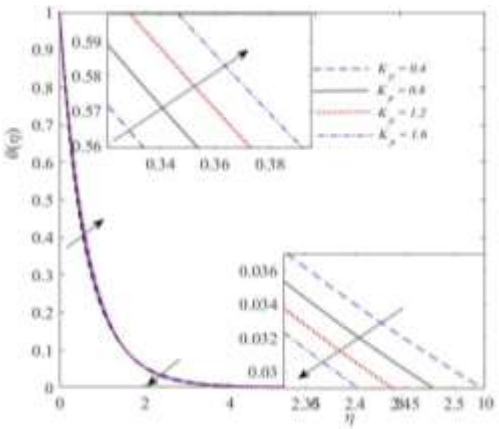

Fig. 9: Variation of $\theta(\eta)$ with Kp.

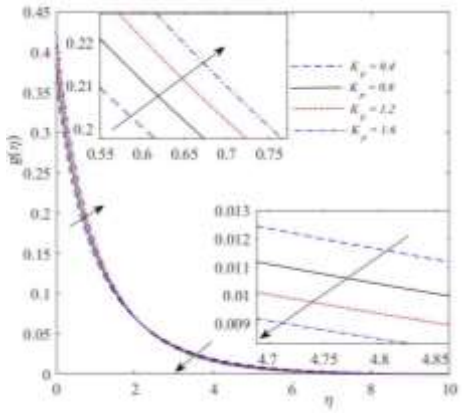

Fig. 10: Variation of $g(\eta)$ with Kp.

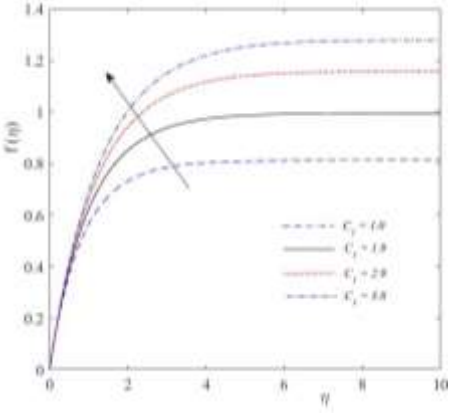

Fig. 11: Variation of $f(\eta)$ with C_1.

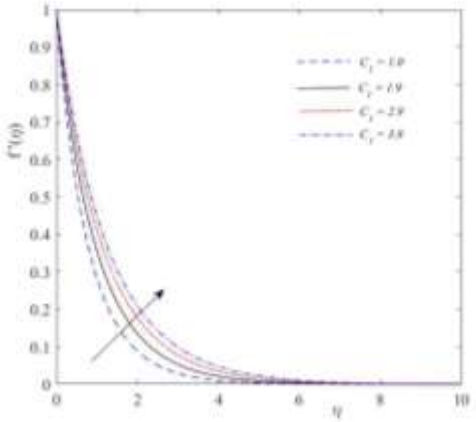

Fig. 12: Variation of $f'(\eta)$ with C_1.

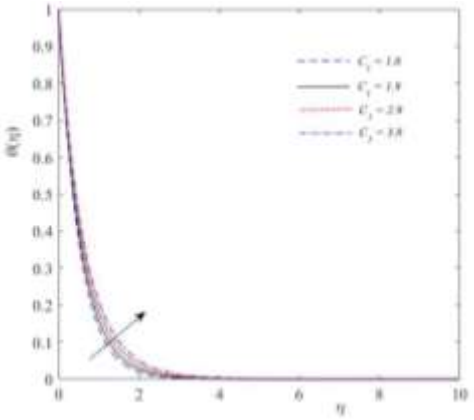

Fig. 13: Variation of $\theta(\eta)$ with C_1.

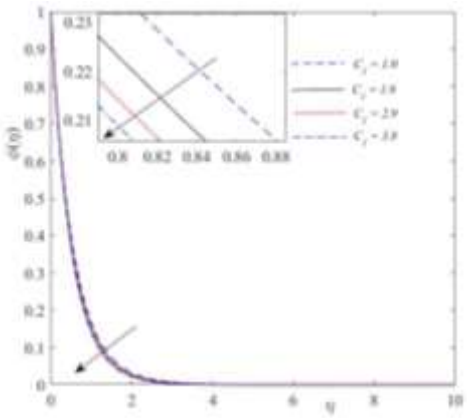

Fig. 14: Variation of $\phi(\eta)$ with C_1.

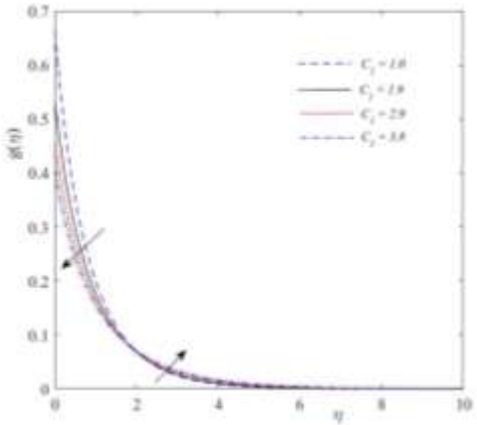

Fig. 15: Variation of $g(\eta)$ with C_1.

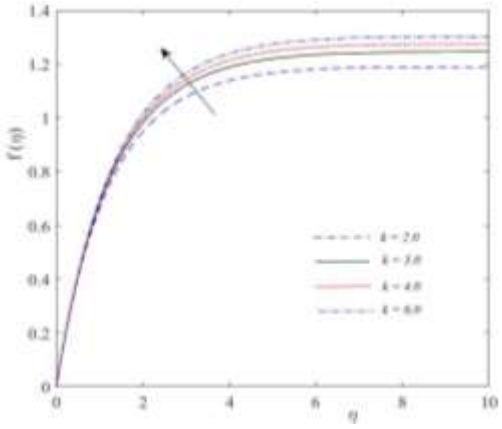

Fig. 16: Variation of $f(\eta)$ with k.

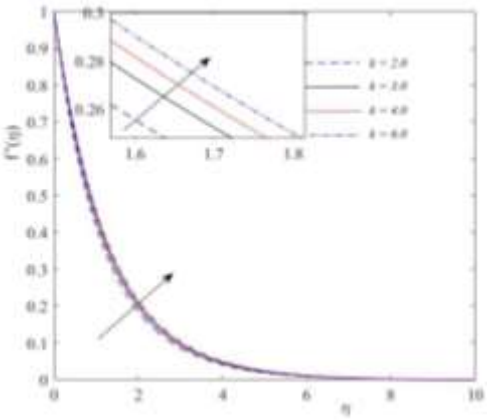

Fig. 17: Variation of $f'(\eta)$ with k.

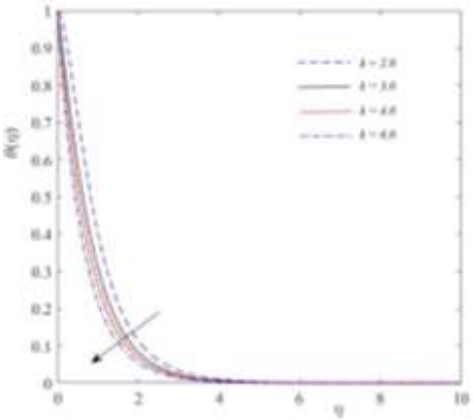

Fig. 18: Variation of $\theta(\eta)$ with k.

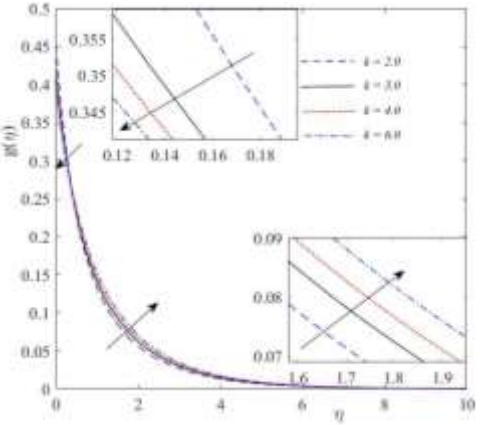

Fig. 19: Variation of $g(\eta)$ with k.

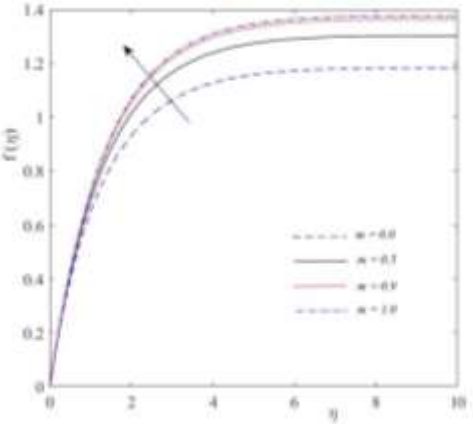

Fig. 20: Variation of $f(\eta)$ with m.

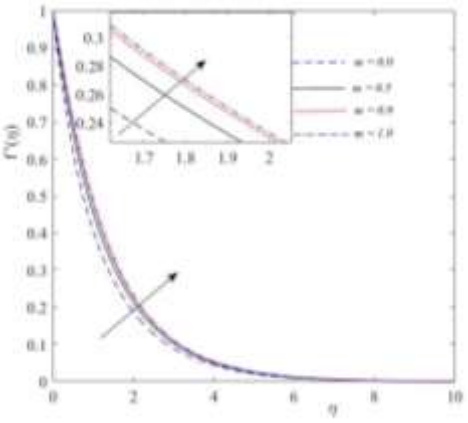

Fig. 21: Variation of $f'(\eta)$ with m.

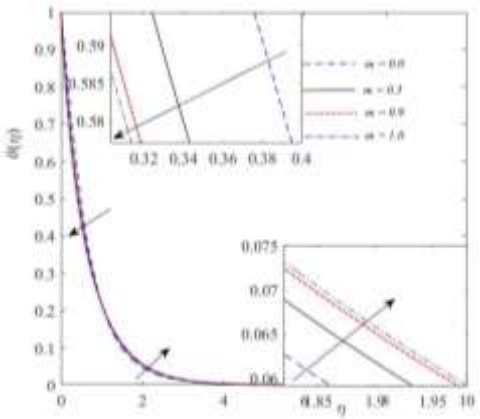

Fig. 22: Variation of $\theta(\eta)$ with m.

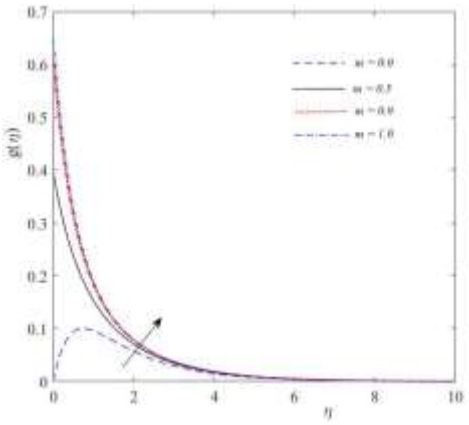

Fig. 23: Variation of $g(\eta)$ with m.

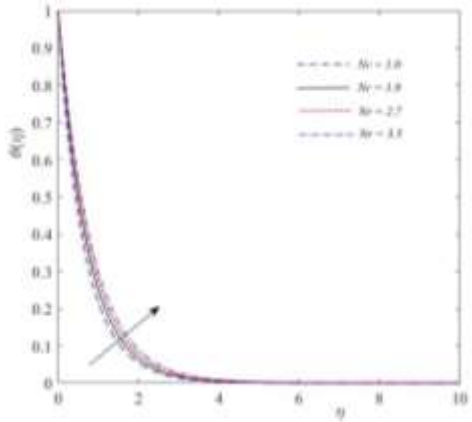

Fig. 24: Variation of $\theta(\eta)$ with Nr.

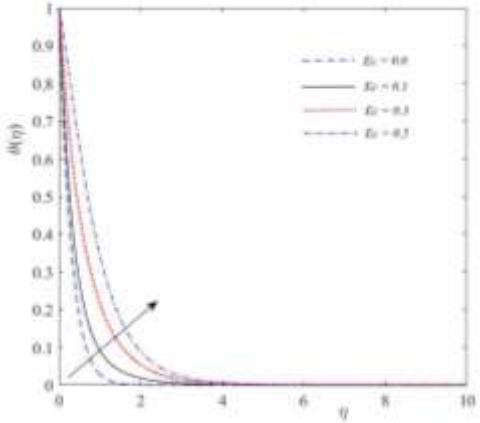

Fig. 25: Variation of $\theta(\eta)$ with Ec.

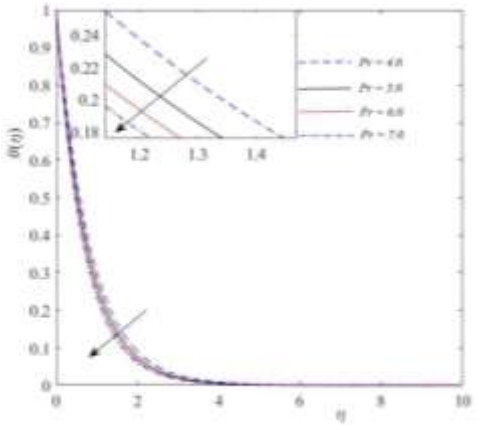

Fig. 26: Variation of $\theta(\eta)$ with $\Pr$.

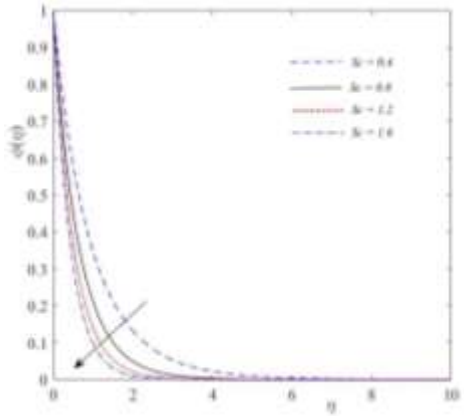

Fig. 27: Variation of $\phi(\eta)$ with Sc.

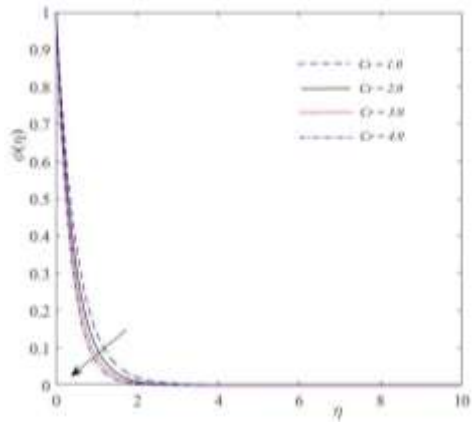

Fig. 28: Variation of $\phi(\eta)$ with Cr .

Acknowledgement: The authors are thankful to Referee for valuable comments and suggestions.

References

[1] Abbas, Z., Naveed, M. and Sajid, M. (2013). Heat transfer analysis for stretching flow over curved surface with magnetic field, *Journal of Engineering Thermophysics*, **22**(4), 337–345. https://doi.org/10.1134/s1810232813040061.

[2] Abbas, N., Rehman, K.U., Shatanawi, W. and Al-Eid, A.A. (2022). Theoretical study of non-Newtonian micropolar nanofluid flow over an exponentially stretching surface with free stream velocity, *Advances in Mechanical Engineering*, **14**(7), 1-9. https://doi.org/10.1177/16878132221107790.

[3] Abbas, N., Shatanawi, W. and Shatnawi, T.A.M. (2024). Thermodynamic properties of Casson-Sutterby-Micropolar fluid flow over exponential stretching curved sheet with impact of MHD and heat generation, *Case Studies in Thermal Engineering*, **55**, 1-15. https://doi.org/10.1016/j.csite.2024.104123.

[4] Abd El-Aziz, M. (2013). Mixed convection flow of a Micropolar fluid from an unsteady stretching surface with viscous dissipation. *Journal of the Egyptian Mathematical Society*, **21(3)**, 385-394. https://doi.org/10.1016/j.joems.2013.02.010.

[5] Ahmed, K., Akbar, T., Muhammad, T. and Alghamdi, M. (2021). Heat transfer characteristics of MHD flow of Williamson nanofluid over an exponential permeable stretching curved surface with variable thermal conductivity. *Case Studies in Thermal Engineering*, **28**, 1-14. https://doi.org/10.1016/j.csite.2021.101544.

[6] Amjad, M., Zehra, I., Nadeem, S. and Abbas, N. (2020). Thermal analysis of Casson micropolar nanofluid flow over a permeable curved stretching surface under the stagnation region. *Journal of Thermal Analysis and Calorimetry*, **143**, 2485-2497. https://doi.org/10.1007/s10973-020-10127-w.

[7] Chandrakala, P. and Rao, V.S. (2024). Effect of heat and mass transfer over mixed convective hybrid nanofluids past an exponentially stretching sheet. *CFD Letters*, **16**, 125-140. https://doi.org/10.37934/cfdl.16.3.1251404123.

[8] Char, M. and Chang, C.L. (1995). Laminar free convection flow of Micropolar fluids from a curved surface. *Journal of Physics D: Applied Physics*, **28**, 1324-1331. http://doi.org/10.1088/0022-3727/28/7/008.

[9] Eringen, A.C. (1966). Theory of Micropolar fluids, *Journal of Mathematics and Mechanics*, **16**, 1-18.

[10] Hayat, T., Rashid, M, Imtiaz, M. and Alsaedi, A. (2016). MHD convective flow due to a curved surface with thermal radiation and chemical reaction, *Journal of Molecular Liquids*, 1-15. https://doi.org/10.1016/j.molliq.2016.11.096.

[11] Hayat, A., Sajjad, R., Ellahi, R., Saedi, A. A. and Muhammad, T. (2017). Homogeneous-heterogeneous reactions in MHD flow of Micropolar fluid by a curved stretching surface. *Journal of Molecular Liquids*, 1-20. https://doi.org/ 10.1016/j.molliq.2017.05.054

[12] Hussain, M., Ashraf, M., Nadeem, S. and Khan, M. (2013). Radiation effects on the thermal boundary layer flow of a Micropolar fluid towards a permeable stretching sheet. *Journal of the Franklin Institute*, **350**, 194-210. https://doi.org/10. 1016/j.jfranklin.2012.07.005.

[13] Islam, S., Jawad, M., Gokul, K.C., Zubair, M., Alrabaiah, H., Shah, Z., Khan, W. and Saeed, A. (2020). Entropy optimization in MHD nanofluid flow over a curved exponentially stretching surface with binary chemical reaction and Arrhenius activation energy. *Journal of Physics Communication*, **4**, 1-24. https://doi.org/10.1088/2399- 6528/aba635.

[14] Jamshed, W., Devi S, S.M., Goodarzi, M., Prakash, M., Nisar, K.S., Zakarya, M. and Abdel-Aty, A.H. (2021). Evaluating the unsteady Casson nanofluid over a stretching sheet with solar thermal radiation: An optimal case study. *Case Studies in Thermal Engineering*, **26**,1-15. https://doi.org/10.1016/j.csite.2021.101160.

[15] Jawad, M., Anwar Saeed, A., Gul, T. and Khan, A. (2021). The magnetohydrodynamic flow of a nanofluid over a curved exponentially stretching surface. *Heat Transfer*, 1-24. https://doi.org/10.1002/htj.22127.

[16] Khan, A. A., Khan, M. N., Ahammad, N. A., Ashraf, M., Guedri, K. and Galal, A. M. (2022). Flow investigation of second grade micropolar nanofluid with porous medium over an exponentially stretching sheet. *Journal of Applied Biomaterials and Functional Materials*, 1-12. https://doi.org/10.1177/ 22808000221089782.

[17] Kumar, K.A., Sugunamma, V. and Sandeep, N. (2020). Effect of thermal radiation on MHD Casson fluid flow over an exponentially stretching curved

sheet. *Journal of Thermal Analysis and Calorimetry*, **140**, 2377-2385. https://doi.org/10.1007/s10973- 019-08977-0.

[18] Kumar, K.A., Sugunamma, V., Sandeep, N. and Sivaiah, S. (2020). Physical aspects on MHD Micropolar fluid flow past an exponentially stretching curved surface. *Defect and Diffusion Forum*, **401**, 79-91.

[19] Mohanty, B., Mishra, S.R. and Pattanayak, H.B. (2015). Numerical investigation on heat and mass transfer effect of Micropolar fluid over a stretching sheet through porous media. *Alexandria Engineering Journal*, **54(2)**, 223–232. https://doi.org/10.1016/j.aej.2015. 03.010.

[20] Murtaza, M.G., Begum, J., Tzirtzilakis, E.E. and Ferdows, M. (2023). MHD flow and heat transfer of water-based nanofluid passing a permeable exponentially shrinking sheet with thermal radiation. *Contemporary Mathematics*, **4**, 358-378. https://doi.org/10. 37256/cm.4220232684.

[21] Nabwey, H.A., Rashad, A.M., Khan, W.A., El-Kabeir, S.M.M. and Elnaem, S.A. (2023). Heat transfer in MHD flow of Carreau ternary-hybrid nanofluid over a curved surface stretched exponentially. *Frontiers in Physics*, **11**, 1-14. https://doi.org/10.3389/fphy. 2023.1212715.

[22] Nagaraja, B. and Gireesha, B.J. (2020). Exponential space-dependent heat generation impact on MHD convective flow of Casson fluid over a curved stretching sheet with chemical reaction. *Journal of Thermal Analysis and Calorimetry*. https://doi.org/ 10.1007/s10973-020-09360-0.

[23] Naveed, M., Abbas, Z. and Sajid, M. (2016). MHD flow of Micropolar fluid due to a curved stretching sheet with thermal radiation. *Journal of Applied Fluid Mechanics*, **9**,131-138.

[24] Oke, A.S., Prasannakumara, B.C., Mutuku, W.N., Punith Gowda, B.A., Juma, B.A., Kumar, R.N. and Bada, O.I. (2022). Exploration of the effects of Coriolis force and thermal radiation on water-based hybrid nanofluid flow over an exponentially stretching plate, *Scientific Reports*, **12**, 1-13. https://doi.org/ 10.1038/s41598-022-21799-9.

[25] Pasha, P., Mirazaei, S. and Zarinfar, M. (2022). Application of numerical methods in Micropolar fluid flow and heat transfer in permeable plates. *Alexandria Engineering Journal*, **61**, 2663-2672.

[26] Qian, W., Khan, M.I., Shah, F., Khan, M., Chu, Y., Khan, W.A. and Nazeer, M. (2021). Mathematical modeling and MHD flow of Micropolar fluid toward an exponential curved surface: Heat analysis via ohmic heating and heat source/sink. *Arabian Journal for Science and Engineering*.

[27] Raju, C.S.K., Sandeep, N., Sugunamma, V., Babu, M.J. and Reddy, J.V.R. (2015). Heat and mass transfer in magnetohydrodynamic Casson fluid over an

exponentially permeable stretching surface. *Engineering Science and Technology, an International Journal*, 1-8. http://doi.org/10.1016/ j.jestch.2015.05.010.

[28] Rees, D.A.S. and Bassom, A.P. (1996). The Blasius boundary-layer flow of a Micropolar fluid. *International Journal of Engineering Science*, **34**(1), 113–124. https://doi.org/ 10.1016/0020-7225(95)00058-5.

[29] Reddy, N.N., Rao, V.S. and Reddy, B.R. (2021), Chemical reaction impact on MHD natural convection flow through porous medium past an exponentially stretching sheet in presence of heat source/sink and viscous dissipation. *Case Studies in Thermal Engineering*, **25**, 1-10. https://doi.org/10.1016/ j.csite.2021.100879.

[30] Sajid, M., Ali, N., Abbas, Z. and Javed, T. (2011). Flow of a Micropolar fluid over a curved stretching surface. *Journal of Engineering Physics and Thermophysics*, **84**(4), 864-871. https://doi.org/10.1007/s10891-011-0544-2.

[31] Sajid, M., Ali, N., Javed, T. and Abbas, Z. (2010). Stretching a curved surface in a viscous fluid. *Chinese Physics Letters*, **27**(2), 1-4.

[32] Sakiadis, B.C. (1961). Boundary layer behavior on continuous solid surface. *AICHE Journal*, **7**(1), 26-28.

[33] Saleh, S.H.M., Arifin, N.M., Nazar, R. and Pop, I. (2017). Unsteady Micropolar fluid over a permeable curved stretching /shrinking Surface. *Hindawi Mathematical Problems in Engineering*, **17**, 1-13. https://doi.org/10.1155/2017/ 3085249.

[34] Sanni, K.M., Saliu, A. and S. Asghar, S. (2024). Heat and mass transport of an advection-diffusion viscous fluid past a magnetized multi-physical curved stretching sheet with chemical reaction. *Mathematical and Computer Modeling of Dynamical Systems*, **30**,131-155. https://doi.org/10.1080/13873954.2024.2311392.

[35] Shabbir, Y., Mushtaq, M., Khan, M.I. and Hayat, T. (2019). Modeling and numerical simulation of Micropolar fluid over a curved surface: Keller Box Method. *Computer Methods and Programs in Biomedicine*, 1-23. https://doi.org/10.1016/j.cmpb.2019.105220.

[36] Shi, Q.H., Shabbir, T., Mushtaq, M., Khan, M.I., Shah, Z. and Kumam, P. (2021). Modelling and numerical computation for flow of Micropolar fluid towards an exponential curved surface: A Keller Box Method. *Scientific Reports*, **11**.

[37] Sidahmed, A.O.M., Salah, F. and Viswanathan, K.K. (2024). Impact of chemical reaction on the Cattaneo-Christov heat flux model for viscoelastic flow over an exponentially stretching sheet. *Scientific Reports*, **14**, 1-14. https://doi.org/ 10.1038/s41598-024-65642-9.

[38] Yasmin, A., Ali, K. and Ashraf, M. (2020). Study of heat and mass transfer in MHD flow of Micropolar fluid over a curved stretching sheet. *Scientific Reports*, **10**, 4581-4591.

[39] Zainal, N.A., Nazara, R., Naganthran, K. and Pop, I. (2021). Unsteady MHD stagnation point flow induced by exponentially permeable stretching/shrinking sheet of hybrid nanofluid, *Engineering Science and Technology, an International Journal*, **24**, 1201-1210. https://doi.org/10.1016/j.jestch.2021.01.018.

[40] Zangooee, M.R., Hosseinzadeh, K. and Ganj, D.D. (2022). Investigation of three-dimensional hybrid nanofluid flow affected by nonuniform MHD over exponential stretching/shrinking plate. *Nonlinear Engineering*, **11**, 143-155. https://doi.org/10.1515/ nleng-2022-0019.

[41] Zeeshan, Ahammad, N.A. and Chung, J.D. (2023). Role of nanofluid and hybrid nanofluid for enhancing thermal conductivity towards exponentially stretching curve with modified Fourier law inspired by melting heat effect, *Mathematics*, **11**, 1-21. https://doi.org/10.3390/math11051170.